

ARMY RESEARCH LABORATORY



Modeling and Design of Mixed-coherence Optical Stacks

by William Beck

ARL-TR-6137

September 2012

NOTICES

Disclaimers

The findings in this report are not to be construed as an official Department of the Army position unless so designated by other authorized documents.

Citation of manufacturer's or trade names does not constitute an official endorsement or approval of the use thereof.

Destroy this report when it is no longer needed. Do not return it to the originator.

Army Research Laboratory

Adelphi, MD 20783-1197

ARL-TR-6137

September 2012

Modeling and Design of Mixed-coherence Optical Stacks

William Beck

Sensors and Electron Devices Directorate, ARL

REPORT DOCUMENTATION PAGE

Form Approved
OMB No. 0704-0188

Public reporting burden for this collection of information is estimated to average 1 hour per response, including the time for reviewing instructions, searching existing data sources, gathering and maintaining the data needed, and completing and reviewing the collection information. Send comments regarding this burden estimate or any other aspect of this collection of information, including suggestions for reducing the burden, to Department of Defense, Washington Headquarters Services, Directorate for Information Operations and Reports (0704-0188), 1215 Jefferson Davis Highway, Suite 1204, Arlington, VA 22202-4302. Respondents should be aware that notwithstanding any other provision of law, no person shall be subject to any penalty for failing to comply with a collection of information if it does not display a currently valid OMB control number.

PLEASE DO NOT RETURN YOUR FORM TO THE ABOVE ADDRESS.

1. REPORT DATE (DD-MM-YYYY) September 2012		2. REPORT TYPE Final		3. DATES COVERED (From - To) September 2011 to August 2012	
4. TITLE AND SUBTITLE Modeling and Design of Mixed-coherence Optical Stacks				5a. CONTRACT NUMBER	
				5b. GRANT NUMBER	
				5c. PROGRAM ELEMENT NUMBER	
6. AUTHOR(S) William Beck				5d. PROJECT NUMBER	
				5e. TASK NUMBER	
				5f. WORK UNIT NUMBER	
7. PERFORMING ORGANIZATION NAME(S) AND ADDRESS(ES) U.S. Army Research Laboratory ATTN: RDRL-SEE-I 2800 Powder Mill Road Adelphi, MD 20783-1197				8. PERFORMING ORGANIZATION REPORT NUMBER ARL-TR-6137	
9. SPONSORING/MONITORING AGENCY NAME(S) AND ADDRESS(ES)				10. SPONSOR/MONITOR'S ACRONYM(S)	
				11. SPONSOR/MONITOR'S REPORT NUMBER(S)	
12. DISTRIBUTION/AVAILABILITY STATEMENT Approved for public release; distribution unlimited.					
13. SUPPLEMENTARY NOTES					
14. ABSTRACT A Mathematica-based program for designing layered optical structures is described that can compute the optical properties at an arbitrary angle of incidence for stacks containing anisotropic and dispersive materials as well as stacks that contain a mixture of coherent and incoherent sections. The program can be used to calculate the properties of a fully specified optical stack or can be used to optimize some property of the stack by varying the thickness or optical properties of the constituent layers. Examples are provided for optimization of a solar cell that has coherent optical layers deposited on an essentially incoherent substrate.					
15. SUBJECT TERMS Optical stack multi-layer coherence transfer-matrix					
16. SECURITY CLASSIFICATION OF:			17. LIMITATION OF ABSTRACT UU	18. NUMBER OF PAGES 24	19a. NAME OF RESPONSIBLE PERSON William Beck
a. REPORT Unclassified	b. ABSTRACT Unclassified	c. THIS PAGE Unclassified			19b. TELEPHONE NUMBER (Include area code) (301) 394-2085

Contents

List of Figures	iv
Acknowledgments	v
1. Introduction	1
2. Design and Modeling Method	3
2.1 4x4 Matrix Method.....	3
2.2 Mixed Coherence	5
2.2.1 Overview	5
2.2.2 Mixed Coherence	5
2.3 Dispersive Index Functions	6
2.4 Determining Absorption in each Layer	7
2.5 Structure Optimization	7
2.6 Efficient Computation	8
3. Example: Optimization of a GaAs Solar Cell Design	8
3.1 Overview	8
3.2 Optimization of Antireflection Coating	9
3.3 Enhancement of QD Absorption by Bragg Reflector	11
4. Conclusion	12
5. References	14
List of Symbols, Abbreviations, and Acronyms	15
Distribution List	16

List of Figures

Figure 1. Calculated transmission for a 200-nm CaF_2 layer on a 100- μm quartz substrate assuming coherent propagation in all layers.	1
Figure 2. Measured transmission for the structure modeled in figure 1.	2
Figure 3. Imaginary part of refractive index (corresponding to absorption) for GaAs (blue) and QD-GaAs (purple).	9
Figure 4. Basic structure of GaAs solar cell with 2-layer AR coating.	9
Figure 5. Solar power spectrum. The purple shaded area is the largest component that can be absorbed in GaAs.	10
Figure 6. Calculated reflection for an AR-coated structure with 2- μm -thick GaAs on top of a 10-period Bragg reflector.	11
Figure 7. Absorption efficiency with Bragg reflector under plain GaAs and QD-enhanced GaAs layer.	12

Acknowledgments

I offer my thanks to Kimberly Sablon-Ramsey and John Little for the design of the gallium arsenide (GaAs) solar cells and for many helpful discussions about their operation. Thanks also go to Kimberly Olver for all of the measured data.

INTENTIONALLY LEFT BLANK.

1. Introduction

Multilayer optical structures are used in a wide variety of devices including photodetectors, lasers, and antireflection (AR) coatings on lenses. The optical properties are typically calculated using a transfer matrix method, which matches the tangential components of the electric and magnetic field at the interfaces between the layers. A method using 2x2 matrices provides a full vector solution for isotropic materials, while Yeh's (1) 4x4 matrix method can be used for birefringent materials.

However, most optical transfer matrix methods assume that light propagates coherently through the structures, i.e., that the phase of the light changes in a fully predictable manner as the light propagates through the layers and across the layer interfaces. This coherent propagation leads to interference oscillations in the reflection and transmission of the stack. However, some of the interference oscillations predicted by the coherent model are not observed in experiments. For example, figure 1 shows the calculated transmission for a 200-nm calcium fluoride (CaF_2) layer on a 100- μm -thick quartz substrate. The low-frequency oscillations are associated with interference in the CaF_2 layer and the high-frequency oscillations are associated with the substrate, but the measured transmission (figure 2) does not contain the high-frequency oscillations.

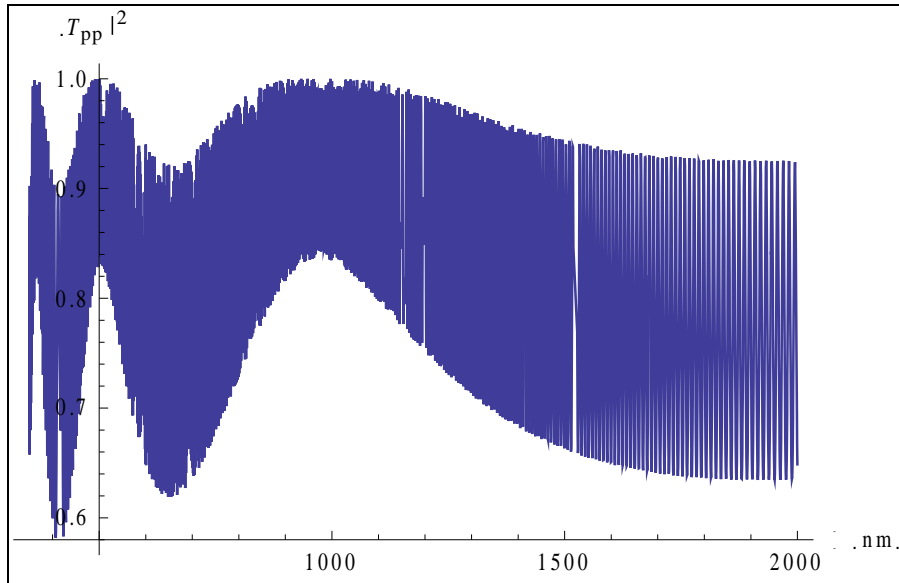


Figure 1. Calculated transmission for a 200-nm CaF_2 layer on a 100- μm quartz substrate assuming coherent propagation in all layers.

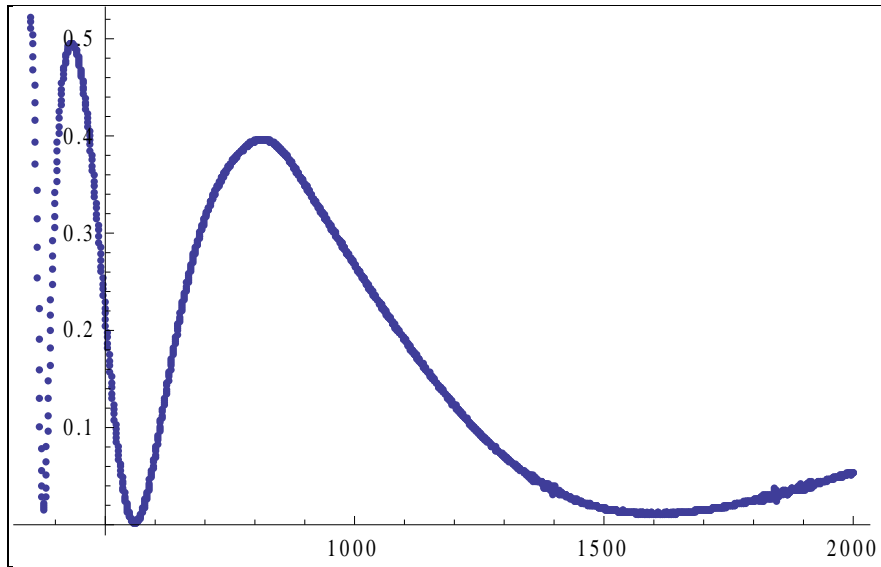


Figure 2. Measured transmission for the structure modeled in figure 1.

The absence of interference oscillations from thicker substrates is typically due to variations in the thickness of the substrate that are larger than the wavelength of the light. Interference can also be suppressed by a rough surface on the back of the substrate. In both cases, the light that is reflected from the back surface arrives at the front surface with a randomized phase, so that the interference predicted by the purely coherent model does not occur. Therefore, it is desirable to have a calculation that properly describes the incoherence and yields results that more closely match experiments. In an ideal case, the calculation would include the ability to describe *partial* coherence, which could treat cases in which the phase of the light is only partially randomized by transmission through a layer or interface. However, partial coherence is more complicated to describe and usually requires Monte Carlo calculations (2) that average over a large set of random phase changes. This makes them slow and generally unsuitable for use in structure optimization, which requires many runs. The model reported here assumes that layers and interfaces are either fully coherent or fully incoherent.

Many of the structures that we would like to model include materials that have a large variation of their refractive indices over the wavelengths of interest. This is particularly true for semiconductor layers, whose absorption drops to nearly zero at wavelengths longer than their cutoff wavelength. Any realistic model should include this variation and provide a variety of tools for specifying the wavelength-dependent complex refractive index.

While it is useful to be able to compute the optical properties of a fully specified structure, it is even more useful to be able to determine the dimensions or materials that optimize some property of the structure. For example, when designing an AR coating for a photodetector that is detecting a laser, the designer would like to determine the AR layer thicknesses that yield the minimum reflection at the laser wavelength. But when designing a broad-band solar cell, the program should maximize the overall solar cell efficiency.

2. Design and Modeling Method

The model that has been implemented uses the Yeh 4x4 matrix method, which provides a full vector electromagnetic solution at any angle of incidence for coherent stacks of isotropic or birefringent materials, but it generalizes that method to accommodate stacks that contain an arbitrary mixture of coherent and incoherent layers and interfaces. The complex refractive indices of all materials are specified by user-definable functions of wavelength, so that arbitrary dispersive properties can be included. Further, the thickness and optical properties of all layers can be specified using variables that are then varied to maximize a user-specified merit function.

2.1 4x4 Matrix Method

The details of the 4x4 matrix method are provided in section 9.7 of Yeh's book (*I*) and are not repeated here, but some of the essential features are described in this section.

In *isotropic* layered media, the electromagnetic radiation can be divided into two uncoupled modes: s modes with an electric field vector perpendicular to the plane of incidence and p modes with an electric field parallel to the plane of incidence. In the case of birefringent layered media, the s and p modes are mixed, but the radiation can be represented by four partial waves, each with a wavevector k_z , electric field polarization vector \mathbf{p} , and magnetic field polarization vector \mathbf{q} that can be calculated from the birefringent material properties. If the four k_z are all real, then two modes have group velocities to the left and the other two have group velocities to the right.

Therefore, the optical field at any point in a layer i can be represented by a vector whose elements are the amplitudes of the four modes. The components of the tangential electric (\mathbf{E}) and magnetic (\mathbf{H}) fields are related to the amplitudes (\mathbf{A}) in the four-component mode vector by a D -matrix such that

$$\begin{pmatrix} E_x \\ H_y \\ E_y \\ H_x \end{pmatrix} = D_i \begin{pmatrix} A_1 \\ A_2 \\ A_3 \\ A_4 \end{pmatrix}_i \quad (1)$$

Therefore, the tangential fields in layer $(i-1)$ can be matched to the fields in layer i by

$$\begin{pmatrix} A_1 \\ A_2 \\ A_3 \\ A_4 \end{pmatrix}_{i-1} = D_{i-1}^{-1} D_i \begin{pmatrix} A_1 \\ A_2 \\ A_3 \\ A_4 \end{pmatrix}_i, \quad (2)$$

where $D_{i-1}^{-1}D_i$ is called the dynamical matrix that relates the mode amplitudes in layer i to the mode amplitudes in the adjacent layer ($i-1$).

Within a layer, the mode amplitudes change exponentially so that the amplitudes at the left side of a layer are related to those at the right side by

$$\begin{pmatrix} A_1 \\ A_2 \\ A_3 \\ A_4 \end{pmatrix}_{i,left} = \begin{pmatrix} \exp[ik_{z1}t] & 0 & 0 & 0 \\ 0 & \exp[ik_{z2}t] & 0 & 0 \\ 0 & 0 & \exp[ik_{z3}t] & 0 \\ 0 & 0 & 0 & \exp[ik_{z4}t] \end{pmatrix}_i \begin{pmatrix} A_1 \\ A_2 \\ A_3 \\ A_4 \end{pmatrix}_{i,right} = P_i \begin{pmatrix} A_1 \\ A_2 \\ A_3 \\ A_4 \end{pmatrix}_{i,right}, \quad (3)$$

where P_i is the propagation matrix for layer i .

The transfer matrix to propagate the mode vector through a stack of layers can be obtained by stringing together the dynamical and propagation matrices for each layer

$$M = D_0^{-1}(D_1P_1D_1^{-1})(D_2P_2D_2^{-1})(D_3P_3D_3^{-1})\dots D_n \quad (4)$$

If the stack is sandwiched between two isotropic media, the modes in the end sections are left- and right-moving s- and p-waves. Assume that the light is incident from the left and let A_s, A_p, B_s, B_p and C_s, C_p be the incident, reflected, and transmitted waves, respectively. Then

$$\begin{pmatrix} A_s \\ B_s \\ A_p \\ B_p \end{pmatrix} = \begin{pmatrix} M_{11} & M_{12} & M_{13} & M_{14} \\ M_{21} & M_{22} & M_{23} & M_{24} \\ M_{31} & M_{32} & M_{33} & M_{34} \\ M_{41} & M_{42} & M_{43} & M_{44} \end{pmatrix}_i \begin{pmatrix} C_s \\ 0 \\ C_p \\ 0 \end{pmatrix}, \quad (5)$$

and the reflection and transmission coefficients can be expressed in terms of the transfer matrix elements by eight relations, including these four examples

$$r_{ss} = \left(\frac{B_s}{A_s} \right)_{A_p=0} = \frac{M_{21}M_{33} - M_{23}M_{31}}{M_{11}M_{33} - M_{13}M_{31}} \quad (6)$$

$$r_{sp} = \left(\frac{B_p}{A_s} \right)_{A_p=0} = \frac{M_{41}M_{33} - M_{43}M_{31}}{M_{11}M_{33} - M_{13}M_{31}} \quad (7)$$

$$t_{ss} = \left(\frac{C_s}{A_s} \right)_{A_p=0} = \frac{M_{33}}{M_{11}M_{33} - M_{13}M_{31}} \quad (8)$$

$$t_{sp} = \left(\frac{C_p}{A_s} \right)_{A_p=0} = \frac{-M_{31}}{M_{11}M_{33} - M_{13}M_{31}}, \quad (9)$$

where the subscripts r and t indicate the modes of the incident and reflected/transmitted waves.

2.2 Mixed Coherence

2.2.1 Overview

As described in section 1, the essential property of a coherent layer or interface is that light propagating through the layer or interface has a predictable phase change based on the thickness and refractive index of the layer or by the change in refractive index across the interface. However, light that propagates through a fully incoherent layer or interface is assumed to emerge with a *random* phase, which is the result of an average over paths with many different phases. In the case of a thick substrate, the random phases are generated by thickness variation within the optical beam area. In the case of an interface, the random phases are typically associated with interface roughness.

An important property of two waves that are *incoherent* is that the total *intensity* is equal to the sum of the two constituent *intensities*. This contrasts with two *coherent* waves, where the total *amplitude* is equal to the sum of the *amplitudes*. The transfer matrices described in section 2.1 are *amplitude* transfer matrices that express the amplitudes on one side of the layer, interface, or stack as a linear combination of the amplitudes on the other side. For example, with

$$\begin{pmatrix} A_1 \\ A_2 \\ A_3 \\ A_4 \end{pmatrix}_L = M \begin{pmatrix} A_1 \\ A_2 \\ A_3 \\ A_4 \end{pmatrix}_R \quad (10)$$

the amplitude of the first component on the left is

$$A_{1L} = M_{11}A_{1R} + M_{12}A_{2R} + M_{13}A_{3R} + M_{14}A_{4R} \quad (11)$$

But if the layer, interface, or stack represented by M is incoherent, the result should express the intensity on the left as an incoherent sum of the individual intensities on the right:

$$|A_{1L}|^2 = |M_{11}|^2 |A_{1R}|^2 + |M_{12}|^2 |A_{2R}|^2 + |M_{13}|^2 |A_{3R}|^2 + |M_{14}|^2 |A_{4R}|^2 \quad (12)$$

It is apparent that the appropriate intensity transfer matrix for an incoherent section is just the amplitude transfer matrix with each element replaced by the square of its absolute amplitude.

2.2.2 Mixed Coherence

A stack comprised of all coherent elements can be modeled using amplitude transfer matrices, and a stack comprised of all incoherent elements can be modeled using intensity transfer matrices. Yet, many real structures contain some coherent and some incoherent elements. For example, when a series of thin layers are deposited onto a thick substrate, the thin layers usually

transmit coherently while the substrate transmits incoherently. A purely coherent analysis of such a structure using amplitude transfer matrices would yield the spurious interference oscillations from the substrate, while a purely incoherent analysis using intensity transfer matrices would eliminate the interference effects that *do* occur in the thin coherent layers. In this case, a mixed analysis must be used in which the coherent sections are first modeled using amplitude transfer matrices and those coherent sections are then incorporated along with the incoherent sections into an analysis by intensity transfer matrices.

The model described in this report first identifies all coherent sub-stacks within the full stack. The amplitude transfer matrix of each sub-stack is calculated using equation 4. Then, those sub-stack amplitude transfer matrices are converted to intensity transfer matrices and combined with the intensity transfer matrices for the incoherent sections to form an overall stack intensity transfer matrix yielding a structure that looks like

$$M_{\text{Intensity}} = \left[\overbrace{\underbrace{D_{air}^{-1} D_1 P_1 D_1^{-1} D_2 P_2 D_2^{-1} D_3 P_3 D_3^{-1} D_s}_{\text{Amplitude Transfer Matrix for Coherent Section}}}^{\text{Intensity Transfer Matrix for Coherent Section}} \right]^2 \overbrace{\left[P_s \right]^2 \left[D_s^{-1} D_{air} \right]^2}^{\text{Incoherent Sections}}, \quad (13)$$

where the numbered subscripts indicate thin coherent layers, and the s subscript indicates an incoherent substrate. The structure could have an arbitrary number of coherent and incoherent sections.

Once the intensity transfer matrix for the whole stack is obtained, we can use intensity versions of equations 5–9 to determine the reflection and transmission coefficients.

2.3 Dispersive Index Functions

The model specifies the complex refractive index in each layer by a user-defined function of wavelength so that arbitrary dispersive properties can be included. Three commonly used functions are the following:

1. A constant function (no dispersion)
2. Interpolation of tabulated experimental data
3. Sellmeier coefficients

The Sellmeier equation (3) is an empirical relationship between refractive index and wavelength for a transparent material that typically provides precise fits to experimental data with a small number of coefficients. A typical form is

$$n^2(\lambda) = 1 + \frac{B_1 \lambda^2}{\lambda^2 - C_1} + \frac{B_2 \lambda^2}{\lambda^2 - C_2} + \frac{B_3 \lambda^2}{\lambda^2 - C_3} + \dots + \frac{B_n \lambda^2}{\lambda^2 - C_n}, \quad (14)$$

where the series is carried out to as few as n=1 or as many as n=5.

In most cases, I have used published Sellmeier coefficients for transparent optical materials such as silicon dioxide (SiO₂), CaF₂, and titanium oxide (TiO₂), and interpolated experimental data for semiconductors such as silicon (Si) and gallium arsenide (GaAs).

2.4 Determining Absorption in each Layer

It is easy to determine the total absorption A in a stack from the reflection R and transmission T coefficients using $A = 1 - R - T$, but in some cases, we need to know the absorption in the individual constituent layers of the stack. Again using a solar cell as an example, the cell may contain a junction area in which absorption leads to photocurrent, but also absorbing contact layers that generate no photocurrent. Knowing the absorption in each individual layer allows us to design the contact layer thickness so that it doesn't absorb a significant fraction of the incident light. We can then choose to optimize the AR coating thicknesses to maximize the absorption in the useful junction region.

The model uses two passes to determine the layer-by-layer absorption. The first pass determines the reflection and transmission coefficients for the full stack. Using these coefficients with equation 5, we see that the right-side intensity vector that corresponds to an incident s-wave from the left side with unit intensity is $(T_{ss} \ 0 \ T_{sp} \ 0)$. The right-side intensity vector corresponding to an incident p-wave from the left side is $(T_{ps} \ 0 \ T_{pp} \ 0)$.

In the second pass, the right-side vector determined in the first pass is propagated through each layer and interface of the stack from right to left, thereby determining the vector at every location in the stack. This then determines the transverse electric and magnetic fields at every location through equation 1. The power flow can then be computed from the z-component of the Poynting vector

$$S_z = \frac{1}{2} \text{Re} [E_x H_y^* - E_y H_x^*] \quad (15)$$

Knowing the power flow at every interface allows us to compute the power lost in each layer, which is the absorption. Note that equation 15 is valid even in absorbing regions with complex k -vector, whereas the more commonly used expression

$$S = \frac{\mathbf{k}}{2\omega\mu} |E|^2 \quad (16)$$

is only valid in regions with real k .

2.5 Structure Optimization

When defining the stack, any of the stack parameters can be left as a variable. The user can then define an arbitrary merit function that depends on the optical coefficients of the stack and use the powerful nonlinear optimization routines that are built into Mathematica to find the values of the

variable parameters that maximize the merit function. The variables can be real numbers, such as the thickness of a layer, but they can also be integers that specify which material to use out of a list of candidate materials. For example, the optimization for an AR coating can determine the best combination of thicknesses *and* material to use. Furthermore, the goal function can include any of the built-in Mathematica functions such as integration and differentiation, so that quite complex optimization problems can be set up.

2.6 Efficient Computation

Execution speed is important for doing structure optimization. For example, if we want to optimize the thicknesses in a multilayer AR coating on a solar cell, we need to maximize the overall solar cell efficiency, which is an integral of the absorption over the full solar wavelength band. So, computing the efficiency for a single AR coating requires computing the transfer matrices and optical coefficients at hundreds of wavelengths. Then, optimizing the AR coating thicknesses requires computing the full spectrum over hundreds, or even thousands, of different combinations of thicknesses.

The most direct way to evaluate the stack transfer matrix shown in equation 4 or 13 is to simply compute the transfer matrix for each layer and interface, in turn, and then multiply them together. However, that method leads to lots of repeated calculation of the same matrices. For example, the D matrices are only a function of the material and the wavelength, so all layers and interfaces that use a particular material have the same D matrix. To maximize execution efficiency, the model first looks through the stack to identify all of the materials that are used. At each wavelength it pre-computes the D matrices and other parameters that only depend on material. By using this approach, as well as similar strategies to reduce duplicated calculations, the execution time was reduced by a factor of 7, reducing the time for solar cell optimizations from more than an hour to 5–10 min (on a Dell Latitude E4300 laptop).

3. Example: Optimization of a GaAs Solar Cell Design

3.1 Overview

This example came out of a project within the Electro-optic (EO)/Infrared (IR) Materials and Devices Branch at the U.S. Army Research Laboratory (ARL) to develop high-performance GaAs-based solar cells for Army applications. GaAs absorbs strongly at wavelengths below its cutoff wavelength of 870 nm, but the solar cell efficiency could be improved by extending the absorption to longer wavelengths by adding layers of quantum dots (QDs), which extend the absorption to roughly 1000 nm. However, as shown in figure 3, the extended absorption yielded by the QDs is relatively weak, so an optical structure was desired to enhance the absorption in the region between 870 and 1000 nm. In addition, we wanted to design an AR coating that would

maximize the solar cell efficiency for plain GaAs structures and also for the wavelength-extended QD-GaAs structures.

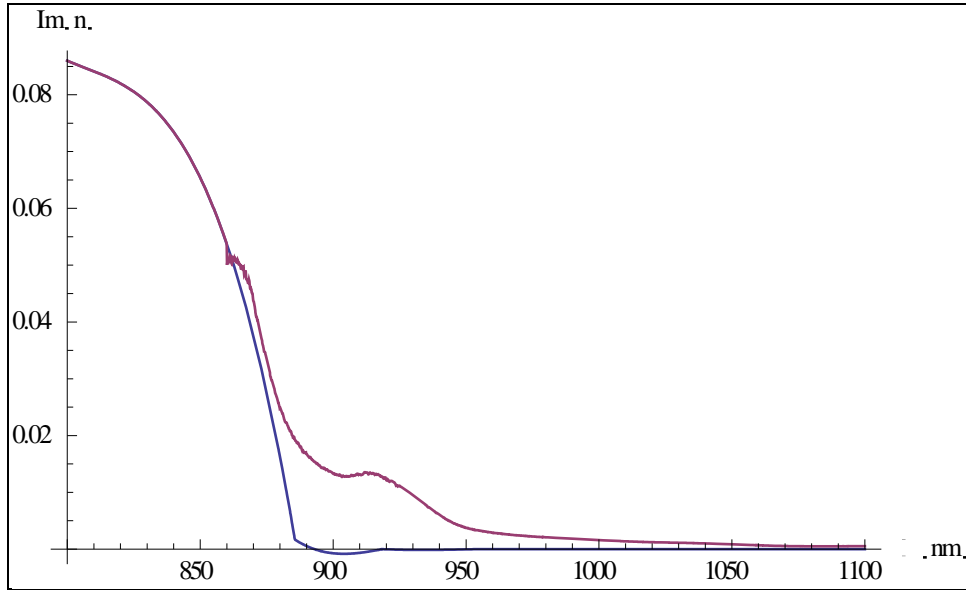


Figure 3. Imaginary part of refractive index (corresponding to absorption) for GaAs (blue) and QD-GaAs (purple).

3.2 Optimization of Antireflection Coating

The basic structure of the plain GaAs solar cell is shown in figure 4. The goal was to choose materials and thicknesses for the AR coating to maximize the solar cell efficiency. The full solar cell efficiency is determined by the efficiency with which the cell converts incident photons into photoelectrons and then the efficiency with which the device extracts those photoelectrons and sends them to an external circuit. This modeling addressed only the first step so the efficiency was defined as the ratio of the power in photo excited carriers divided by the total incident solar power.

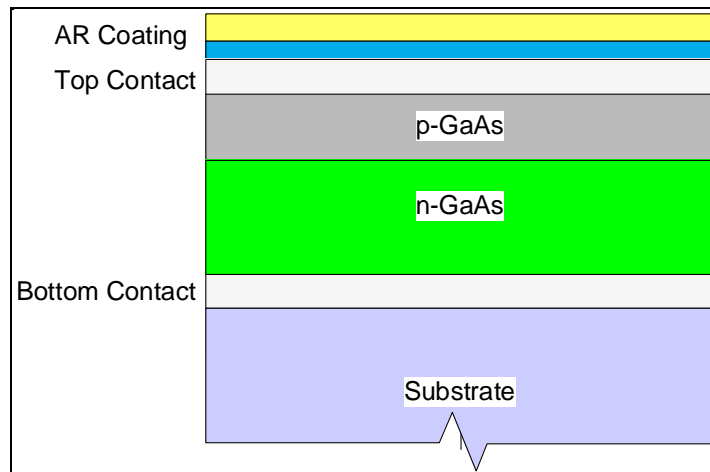


Figure 4. Basic structure of GaAs solar cell with 2-layer AR coating.

The solar power spectrum is shown in figure 5 along with shading indicating the maximum fraction of that power that can be absorbed in GaAs with its cutoff of 870 nm. The actual efficiency will be

$$Eff = \int_0^{\lambda_{cutoff}} S[\lambda]A[\lambda] \frac{\lambda}{\lambda_{cutoff}} d\lambda \bigg/ \int_0^{\lambda_{cutoff}} S[\lambda]d\lambda \quad (17)$$

where $S[\lambda]$ is the solar power spectrum, $A[\lambda]$ is the fraction of incident light absorbed at wavelength λ , and $\lambda / \lambda_{cutoff}$ reflects the fact that when a photon with energy $E_\lambda > E_{gap}$ is absorbed, it generates an excited carrier with energy E_λ that rapidly decays to a carrier with energy E_{gap} , with the excess energy $E_\lambda - E_{gap}$ lost as heat. With this factor included, the maximum efficiency for a GaAs solar cell is 40%. The goal for the optical design was to choose an AR coating that maximized Eff to as close as possible to that theoretical maximum.

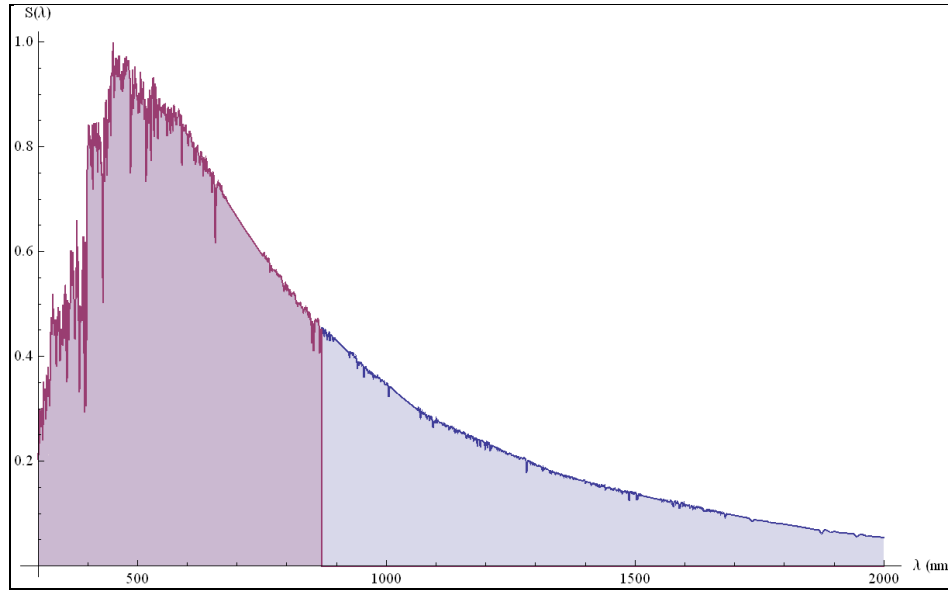


Figure 5. Solar power spectrum. The purple shaded area is the largest component that can be absorbed in GaAs.

An example of one run to find an optimum two-layer AR coating illustrates the process. The calculation used interpolated numerical data for the solar spectrum and the complex refractive index of GaAs. A “menu” of possible transparent materials to use in the AR coating was constructed including yttrium oxide (Y_2O_3), tantalum pentoxide (Ta_2O_5), CaF_2 , magnesium fluoride (MgF_2), SiO_2 , silicon nitride (Si_3N_4), and TiO_2 with the refractive index of each specified by published Sellmeier coefficients. The programmed specification for each layer of the AR coating included an integer variable to specify which material from the “menu” to use and a real variable to specify the thickness of the layer. The GaAs absorbing layer was 2 μm thick. All layers were assumed to be coherent except the substrate, which was incoherent. The

Mathematica optimization routine was then used to find the combination of materials and thicknesses that yielded the largest value of Eff in equation 17.

After sorting through all of the possible material combinations in the AR coating, the model found that the best result was obtained with 46.33 nm of TiO_2 followed by 89.78 nm of CaF_2 , which yielded an efficiency of 38.6%.

3.3 Enhancement of QD Absorption by Bragg Reflector

The absorption strength of GaAs well below its cutoff is very strong so that nearly all light in that wavelength range is absorbed in a 2- μ m-thick layer. But as shown in figure 3, the extended absorption provided by QDs between 870 and 1000 nm is much weaker, and incident light in that wavelength range is not fully absorbed in a 2- μ m-thick layer. Therefore, the efficiency at those wavelengths should be improved by a back reflector that sends light back through the layer on a second pass. This reflector should be placed between the substrate and the device layers to avoid parasitic absorption of light going through the substrate. The simplest back reflector would be a layer of gold, but gold does not grow epitaxially on GaAs so it cannot be placed between the substrate and other epitaxial layers of the structure. Thus, the structure modeled here used a Bragg reflector consisting of alternating layers of GaAs and $Al_{0.8}Ga_{0.2}As$. The best results were obtained with a reflector consisting of 10-periods of 63-nm GaAs/75-nm $Al_{0.8}Ga_{0.2}As$, which yields a reflection band centered at 900 nm. The strong effect of the reflector can be seen in figure 6, which shows the calculated overall reflection from an AR-coated structure containing a 2- μ m-thick layer of plain GaAs (which does not absorb in the 870–1100 nm region) on top of a 10-period Bragg reflector.

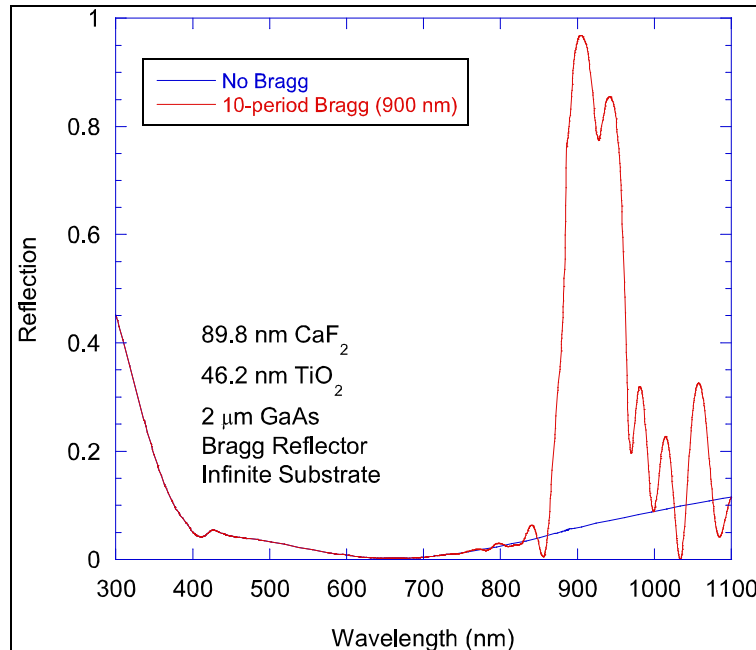


Figure 6. Calculated reflection for an AR-coated structure with 2- μ m-thick GaAs on top of a 10-period Bragg reflector.

When the Bragg reflector is used under a QD-enhanced GaAs layer, it increases the absorption in the QD enhancement region (870–1000 nm) as well as at wavelengths just below the GaAs cutoff where the GaAs absorption is relatively weak. Figure 7 shows the calculated absorption efficiency ($A[\lambda]$ in equation 17) for a simple cell using plain GaAs and no Bragg reflector, QD-enhanced GaAs with no Bragg reflector, and QD-enhanced GaAs with a Bragg reflector. The Bragg reflector nearly doubles the absorption in the QD-enhanced wavelength range. The corresponding solar cell efficiencies were 38.6% for the simple cell, 40.5% for QD-enhanced without Bragg reflector, and 42.1% for QD-enhanced with Bragg reflector.

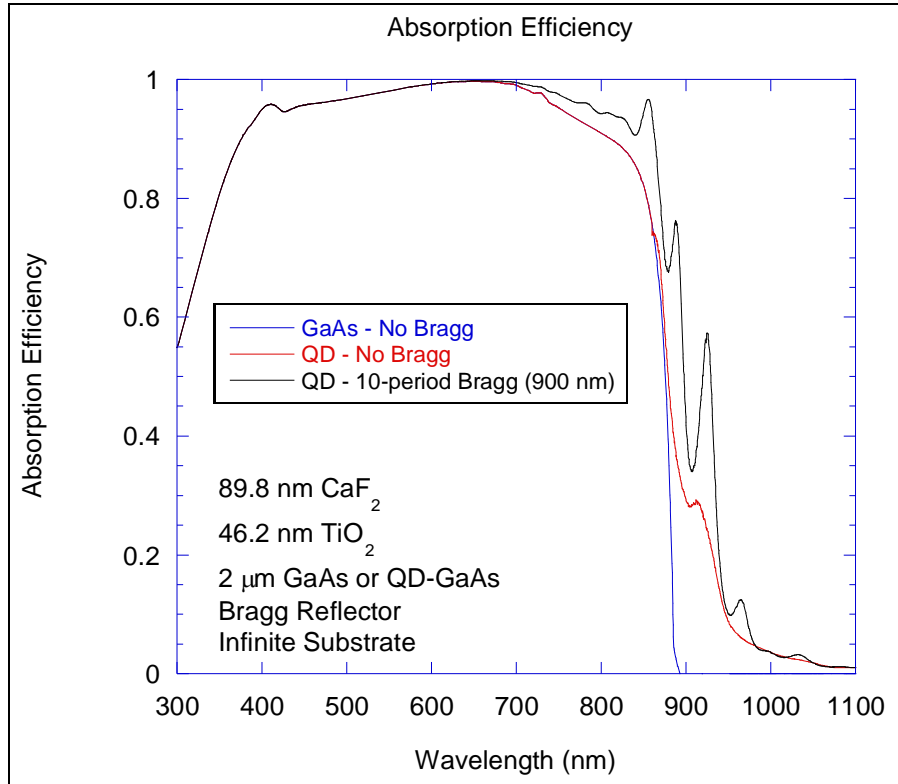


Figure 7. Absorption efficiency with Bragg reflector under plain GaAs and QD-enhanced GaAs layer.

4. Conclusion

The Mathematica model described in this report is a powerful tool for designing layered optical structures. It includes capability for anisotropic (birefringent) materials whose complex refractive index can be defined by arbitrarily complex functions of wavelength. Standard functions are provided for materials defined by Sellmeier coefficients or by interpolating experimental data. Optical properties of the structures can be computed at an arbitrary angle of incidence.

The model can treat structures containing arbitrary combinations of coherent and incoherent layers and interfaces. This eliminates the spurious, high-frequency oscillations in the optical properties of thick incoherent layers that are predicted by purely coherent models while preserving interference effects within the coherent regions.

The model uses the powerful nonlinear optimization capabilities of Mathematica to find the structure dimensions and materials that maximize a user-defined merit function. This capability has been used to design optimized AR coatings and Bragg reflectors for QD-enhanced GaAs solar cells.

5. References

1. Yeh, P. *Optical Waves in Layered Media*; John Wiley & Sons, New York, 1988.
2. Troparevsky, M. C.; Sabau, A. S.; Lupini, A. R.; Zhang, Z. *Optics Express* **2010**, *18* (24), 24715-24721.
3. Wikipedia. *Sellmeier equation*. http://en.wikipedia.org/wiki/Sellmeier_equation (accessed August 26, 2012).

List of Symbols, Abbreviations, and Acronyms

AR	antireflection
ARL	U.S. Army Research Laboratory
CaF ₂	calcium fluoride
EO	electro-optic
GaAs	gallium arsenide
IR	infrared
MgF ₂	magnesium fluoride
QDs	quantum dots
Si	silicon
Si ₃ N ₄	silicon nitride
SiO ₂	silicon dioxide
Ta ₂ O ₅	tantalum pentoxide
TiO ₂	titanium oxide
Y ₂ O ₃	yttrium oxide

NO. OF COPIES	ORGANIZATION
1 ELEC	ADMNSTR DEFNS TECHL INFO CTR ATTN DTIC OCP 8725 JOHN J KINGMAN RD STE 0944 FT BELVOIR VA 22060-6218
1	US ARMY RSRCH DEV AND ENGRG CMND ARMAMENT RSRCH DEV & ENGRG CTR ARMAMENT ENGRG & TECHNLOGY CTR ATTN AMSRD AAR AEF T J MATTS BLDG 305 ABERDEEN PROVING GROUND MD 21005-5001
1	US ARMY INFO SYS ENGRG CMND ATTN AMSEL IE TD A RIVERA FT HUACHUCA AZ 85613-5300
1	US GOVERNMENT PRINT OFF DEPOSITORY RECEIVING SECTION ATTN MAIL STOP IDAD J TATE 732 NORTH CAPITOL ST NW WASHINGTON DC 20402
4	US ARMY RSRCH LAB ATTN IMAL HRA MAIL & RECORDS MGMT ATTN RDRL CIO LL TECHL LIB ATTN RDRL CIO LT TECHL PUB ATTN RDRL SEE I W BECK ADELPHI MD 20783-1197